

Considering lensing effect on gravitational wave signals from black holes in mass gap

Qiyuan Yang,¹ Zhi-Qiang You ² and Xilong Fan ^{1, *}

¹*School of Physics and Technology, Wuhan University, Wuhan 430072, China*

²*Institute for Gravitational Wave Astronomy, Henan Academy of Sciences, Zhengzhou 450046, Henan, China*

(Dated: December 25, 2025)

The pair-instability supernova (PISN) mechanism predicts a mass gap in the black hole population, where no stellar-origin black holes are expected to form. However, the binary black hole merger events GW190521 and GW231123 appear unusual, as current analyses place their component masses within the PISN mass gap. In this work, we investigate the relationship between different lensing magnifications and the inferred source-frame black hole masses for these two events. If the gravitational wave source is lensed, neglecting lensing effect can bias the inferred luminosity distance and hence the redshift, leading to an underestimation of the luminosity distance and consequently an overestimation of the source-frame masses, potentially placing them in the mass-gap region. For the two events in mass gap, when adopting a lower bound of $60M_{\odot}$ for the mass gap, the minimum magnifications required to shift the inferred source-frame masses below this gap boundary are found to be $\mu = 12.2$ for GW190521 and $\mu = 320.1$ for GW231123, corresponding to lensing-corrected luminosity distances of 11155 Mpc and 15207 Mpc, respectively. These results provide a quantitative reference for assessing the lensing hypothesis as a possible explanation for the existence of black holes in the PISN mass gap.

I. INTRODUCTION

Since the first signal GW150914 of gravitational wave (GW) from a binary black hole (BBH) merger was detected by LIGO [1–4], gravitational wave astronomy has opened an entirely new window into the study of black hole (BH) formation and evolution. With the subsequent participation of the Virgo [5] and KAGRA [6–9], the LIGO–Virgo–KAGRA (LVK) network has detected hundreds of BBH merger events up to the latest O4 observing run [10–13].

Among these detections, a subset of sources exhibit unusually large component masses, which challenge our current understanding of stellar evolution and black holes (BHs) formation channels. GW190521 is particularly remarkable [14, 15]. Detected during the second observing run (O2), it was the most massive BBH merger observed at that time, with component masses of approximately $m_1 \approx 98 M_{\odot}$ and $m_2 \approx 57 M_{\odot}$ [16]. This makes it the first event with BH mass falls within the so-called pair-instability supernova (PISN) mass gap [17–19]. The PISN theory predicts that when the helium-core mass of a star lies between the lower boundary of about $45 \sim 60 M_{\odot}$ and the upper boundary of about $120 \sim 150 M_{\odot}$ [20–28], the star undergoes a pair-instability explosion that completely disrupts it, leaving no compact remnant. Therefore, standard stellar evolution models do not expect the formation of BHs within this mass range. GW190521 is thus regarded as the first BBH event with at least one component located inside the PISN mass gap [29, 30]. More recently, another high-mass event, GW231123, was reported during the latest fourth observing run (O4), with component masses of approximately

$m_1 \approx 137 M_{\odot}$ and $m_2 \approx 101 M_{\odot}$ [31]. It represents the most massive BBH event detected so far. Such extreme component masses again far exceed the lower boundary of the PISN mass gap, making GW231123 another potential candidate within this regime. The recurrence of such high-mass events raises a key question: is the upper mass limit of stellar-origin BHs truly as predicted by current theory, or could other astrophysical or observational effects be responsible for the apparent overestimation of masses? The observation of BBH mergers located within the PISN mass gap clearly challenges this traditional picture of BH formation [32].

To explain these high-mass merger events, several possible formation channels have been proposed. One explanation suggests that these high-mass systems may originate from primordial black holes, which form in the early Universe through the collapse of enhanced curvature perturbations rather than stellar evolution [33–38]. Another scenario is that of hierarchical mergers, in which smaller black holes repeatedly merge to gradually form more massive remnants [39–46]. However, these mechanisms typically require special astrophysical conditions and relatively high merger rates, and their overall feasibility remains a subject of ongoing debate [47–52]. In addition, another compelling explanation involves gravitational lensing [53, 54]. If the GW signal produced by a BBH merger is strongly lensed by a galaxy or galaxy cluster located between the source and the observer, the observed strain amplitude will be magnified [55–58]. If the lensing magnification effect is not taken into account, the inferred luminosity distance will be underestimated, leading to an underestimation of the redshift [59–61]. Since the true source-frame masses of the BHs are related to the detector-frame masses through the redshift, an underestimated redshift will result in overestimated source-frame masses, causing them to fall into the PISN mass gap. This effect can naturally explain some of the

* xilong.fan@whu.edu.cn

observed massive BBH events in the mass gap without invoking extreme formation scenarios.

In this work, we investigate whether the observed properties of GW190521 and GW231123 could be affected by gravitational lensing magnification. We simulate GW190521-like and GW231123-like signals and perform parameter estimation (PE) using both unlensed waveform templates and lensed templates under the geometric-optics approximation, as detected by LVK network. This allows us to evaluate whether the lensing effect can cause the inferred source-frame masses to cross the PISN boundary. For these two mass-gap events, larger magnification factors correspond to smaller source-frame masses, enabling them to move out of the mass gap. After determining the magnification corresponding to a given lower boundary of the mass gap, we present the corrected source masses and luminosity distances when lensing effects are taken into account. The results indicate that gravitational lensing effect may play an important role in source parameter inference when interpreting high-mass BBH events.

In the following sections, we first introduce lensing effect in Sec. II and describe how to construct the lensed GW waveform. Then in Sec. III, we introduce Bayesian PE method for lensed BBH GW signal, and apply it to GW190514-like and GW231123-like events. And in Sec. IV we present the results of the selected parameters under unlensed and lensed scenarios for the two events. The summary and discussion of this work is given in Sec. V lastly. In this work, we adopt the Λ CDM cosmology model described in Ref. [62], which is also coded in **Astropy**¹ [63] with assumptions of $H_0 = 67.66 \text{ km} \cdot \text{s}^{-1} \cdot \text{Mpc}^{-1}$, $\Omega_{\text{m}} = 0.30966$, $T_{\text{CMB}} = 2.7255 \text{ K}$.

II. LENSING EFFECT

For an unlensed BBH merger event, the GW waveform h^{ul} can be written as:

$$h^{ul} = F_+ h_+ + F_\times h_\times, \quad (1)$$

where h_+ , h_\times are the two polarization modes of GW and F_+ , F_\times are the antenna pattern functions. h^{ul} is characterized by 15 parameters, which can be divided into two types: 9 intrinsic parameters including BHs masses $m_{1,2}$, spin magnitudes $a_{1,2}$, four angles for spin orientation $\theta_1, \theta_2, \phi_{12}, \phi_{\text{JL}}$, the phase of waveform ϕ , and another 6 extrinsic parameters, which include right-ascension RA, declination DEC, and the luminosity distance d_L , the polarization angle ψ , the angle between line of sight and the total angular momentum θ_{JN} of the GW source, and the time at which the GW merger signal reaches the geocenter t_{geo} .

For the lensed GW, the waveform will be modified by the lensing object. In frequency domain, the relation between a lensed $h^l(f)$ and an unlensed GW waveform $h^{ul}(f)$ is given by [64–66]:

$$h^l(f) = F(f) \cdot h^{ul}(f), \quad (2)$$

where $F(f)$ is the amplification factor, can be given by the diffraction integral:

$$F(f) = \frac{D_s \xi_0^2 (1+z_l)}{D_l D_{ls}} \frac{f}{i} \int e^{2\pi i f t_d(\mathbf{x}, \mathbf{y})} d^2 \mathbf{x}, \quad (3)$$

where D_l , D_s and D_{ls} are the angular diameter distances to the lens, source and from the lens to the source, respectively. z_l is the redshift of lens, ξ_0 is the normalization constant, also represents the physical Einstein radius in the lens plane. t_d is the time delay relative to the straight path in unlensed propagation, determined by the dimensionless position \mathbf{x} in lens plane and \mathbf{y} in source plane. In actual observations, we only care about the relative time delays between different images, so when calculating t_d , we can add an additional phase term to set its minimum value to zero.

If the lens object is a galaxy or galaxy cluster, its physical scale is typically much larger than the wavelength of GW. Therefore, the calculation of the amplification factor can be treated under the geometric optics approximation. For a lensing system that can produce N multiple images, the total amplification factor is [65]:

$$F(f) = \sum_{i=1}^N \sqrt{|\mu_i|} \cdot e^{-i\pi(2f\Delta t_{d_i} + n_i)}, \quad (4)$$

and then the lensed waveform in the frequency domain can be written as:

$$h^l(f) = \sum_{i=1}^N \sqrt{|\mu_i|} \cdot e^{-i\pi(2f\Delta t_{d_i} + n_i)} \cdot h^{ul}(f), \quad (5)$$

where μ_i is the magnification of the i -th image, Δt_{d_i} is the time delay of the i -th image relative to the first one (that means $\Delta t_{d_1} = 0$), and $n_i = 0, \frac{1}{2}, 1$ is called Morse index, when the position of the i -th image is a minimum, saddle, and maximum point of $t_d(\mathbf{x}, \mathbf{y})$, respectively.

Note that the sign in the exponential term of $F(f)$ in this paper differs from Eq. (15) in Ref. [65], because we adopt a Fourier transform convention that is consistent with the one commonly used in GW analyses. Specifically, the inverse Fourier transform convention we adopt is given by:

$$h(t) = \int_{-\infty}^{+\infty} \tilde{h}(f) e^{2\pi i f t} df, \quad (6)$$

then in time domain, the lensed waveform of the i -th image $h_i^l(t)$ is:

$$h_i^l(t) = \sqrt{|\mu_i|} \cdot e^{-i\pi n_i} \cdot h^{ul}(t - \Delta t_{d_i}). \quad (7)$$

¹ <http://www.astropy.org>

This choice of notation ensures consistency with the convention of GW time–frequency transformation. Moreover, the term $h(t - \Delta t_{d_i})$ guarantees that an image with a larger time delay arrives Δt_{d_i} seconds later than the first one, in agreement with actual observational situations.

If we aim to determine properties such as the magnification of a lens, it is necessary to first model the lens. A typical lens model is the singular isothermal sphere (SIS) model, whose Einstein angular radius θ_E is given by:

$$\theta_E = 4\pi \left(\frac{\sigma_v}{c}\right)^2 \frac{D_{ls}}{D_s}, \quad (8)$$

where σ_v is the velocity dispersion of the lens galaxy. When the angular position of the source β is less than θ_E , the SIS lens will produce two images with magnifications μ_+ and μ_- , calculated by:

$$\mu_{\pm} = 1 \pm \frac{1}{y}, \quad (9)$$

here y is the dimensionless source position defined by $y = \beta/\theta_E$. The time delay between two images is:

$$\Delta t_d = \frac{8GM_l(1+z_l)y}{c^3}, \quad (10)$$

where $M_l = \theta_E^2 D_l D_s c^2 / 4D_{ls} G$ is the lens mass inside the Einstein ring. Given a cosmological model, one can calculate D_l , D_s and D_{ls} from the redshift of lens z_l and source z_s . Therefore, for an SIS lens, once the velocity dispersion σ_v and redshift z_l of the lensing galaxy, together with the redshift z_s and angular position β of the source are specified, the relevant lensing parameters can be calculated.

Since the time delay of the first image $\Delta t_{d_1} = 0$ and it is the minimum image of the lens (that means $n_1 = 0$), so for a SIS lens, the lensed GW waveforms $h_1^l(f)$ and $h_2^l(f)$ of the two images are:

$$h_1^l(f) = \sqrt{|\mu_+|} \cdot h^{ul}(f), \quad (11)$$

$$h_2^l(f) = \sqrt{|\mu_-|} \cdot e^{-i\pi(2f\Delta t_d + n_2)} \cdot h^{ul}(f). \quad (12)$$

III. BAYESIAN INFERENCE FOR LENSED BBH

In this section, we employ a Bayesian inference to perform PE on the simulated GW190521-like and GW231123-like signals using both lensed and unlensed templates. For Bayesian PE, we use Bayes' formula to obtain the posterior distribution $p(\theta | d)$ of the parameters θ :

$$p(\theta | d) = \frac{p(d | \theta)p(\theta)}{p(d)}, \quad (13)$$

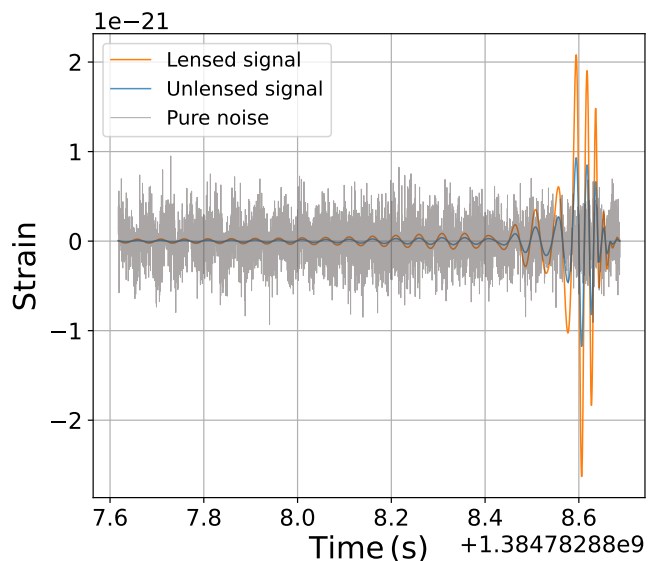


FIG. 1. The amplification effect of GW signal by gravitational lensing. The blue line represent the original GW231123-like signal and orange line represent the first image of the original signal magnificated by a lens with $\mu = 5$ in H1 detector. We also plot the pure noise of the detector, whose strain is nearly comparable to that of the unlensed signal, but is roughly four times smaller than that of the lensed one in merger phase due to the magnification.

where $p(d | \theta)$ is the likelihood function and $p(\theta)$ is the prior. $p(d)$ is the evidence, calculated by the integrate of $p(d | \theta)$ and $p(\theta)$. Usually in GW data analysis, we adopt the standard Gaussian likelihood. In the discrete frequency domain, it can be written as

$$\ln \mathcal{L}(d|\theta) = -\frac{1}{2} \sum_k \left[\frac{|d_k - h_k(\theta)|^2}{\sigma_k^2} + \ln(2\pi\sigma_k^2) \right], \quad (14)$$

where d_k is the detector data, $h_k(\theta)$ is the model waveform evaluated at frequency bin k , and σ_k^2 is the noise variance associated with that bin. The variance is related to the one-sided power spectral density (PSD) $S_n(f)$ via $\sigma_k^2 = \frac{1}{2} S_n(f_k)$. For a given data, using different GW waveform templates $h(\theta)$ will yield different likelihood values and therefore lead to different posterior inferences of the parameters. Consequently, whether the waveform model includes lensing effects can significantly influence the estimation of certain parameters.

Usually, we can obtain the posterior distributions of detector frame masses of each component $m_{1,2}^d$ and the luminosity distance of GW source d_L by Bayesian PE. And the inferred source-frame masses $m_{1,2}$ are constrained by the mass–redshift relation:

$$m_{1,2} = \frac{m_{1,2}^d}{1+z}, \quad (15)$$

where z is the redshift of GW source. Given a cosmological model, one can calculate z from d_L , and then

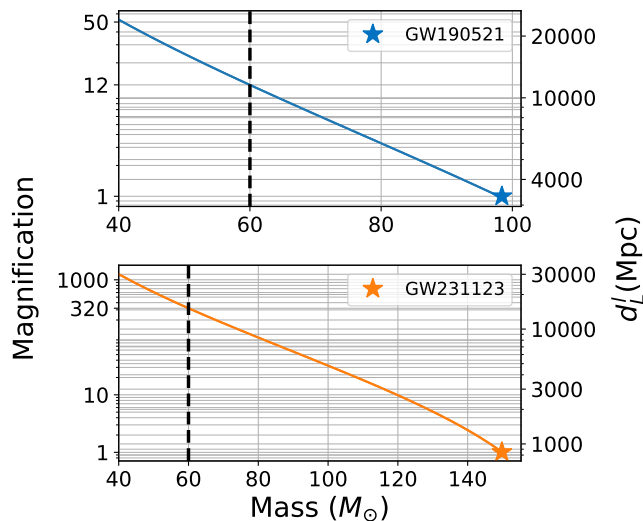


FIG. 2. The relation between the inferred source-frame mass of primary BH (x-axis) and the lensing magnification μ (left y-axis, log scale), together with the corresponding luminosity distance after accounting for the lensing effect d_L^l (right y-axis, log scale). The stars in upper and lower panels correspond to the median value of the posterior samples for real GW190521 and GW231123 events, respectively. And the black dashed line represents the lower boundary of the mass gap $m = 60 M_\odot$ as we take.

calculate $m_{1,2}$. Since the amplitude of GW is inversely proportional to the luminosity distance, through Eq. (11) we can find that the magnification μ of a lensed waveform is degenerate with the luminosity distance. For a given GW signal, the luminosity distances with and without lensing satisfy the following relation:

$$d_L = \frac{d_L^l}{\sqrt{\mu}}, \quad (16)$$

here d_L^l (equal to D_s) denotes the true luminosity distance when considering the lensing effect and d_L is the luminosity distance without lensing. In other words, the lensing effect alters our estimation of the luminosity distance. If a GW signal is lensed, the luminosity distance of GW source inferred under the unlensed scenario will be smaller than the true value, and a smaller luminosity distance means a smaller redshift z . So for a lensed GW event, according to Eq. (15), using an unlensed template will lead to an underestimated luminosity distance, which in turn results in overestimated source-frame masses. Such a biased inference may incorrectly place the event within the mass-gap region, like GW190521 and GW231123. Therefore, it is necessary to employ lensed templates to re-estimate the parameters of such sources.

To perform the Bayesian PE, first we generated GW190521-like and GW231123-like simulated signals us-

ing **Bilby**² [67]. To obtain the original waveforms, we employed the IMRPhenomXPHM [68, 69] model, a state-of-the-art BBH merger waveform that includes inspiral–merger–ringdown phases, higher-order modes and precession, with a sampling frequency of 4096 Hz and a duration of 4 s. We use the median value of the published posterior samples of real GW190514 and GW231123 events from **GWOSC**³ [70] as our injection parameters, which are shown in Table I. Then we injected the signal into the LVK detector network and obtained simulated data. Since no lensing counterparts of these two signals have been identified in current real detections, we only adopt Eq. (11) as our lensed GW template to illustrate the impact of lensing effects on the estimation of source parameters. Using IMRPhenomXPHM as the unlensed template, we construct the lensed GW template according to Eq. (11). As an illustration of the amplification effect by the lens, Fig. 1 shows the signal in H1 detector simulated by both unlensed and lensed templates. The optimal signal-to-noise-ratio (SNR) of the unlensed signal is 34.94, while in the lensed case with a lensing magnification of $\mu = 5$, it is 78.14.

TABLE I. The injection parameters and network optimal SNR of GW190521-like and GW231123-like signals. All these parameters are obtained from the median values of the real posterior samples, estimated by the IMRPhenomXPHM waveform family.

	GW190521-like	GW231123-like
$m_1^d (M_\odot)$	152.4	175.5
$m_2^d (M_\odot)$	89.7	109.4
a_1	0.71	0.79
a_2	0.53	0.68
θ_1 (rad)	2.10	1.81
θ_2 (rad)	1.43	0.85
ϕ_{12} (rad)	3.25	4.39
ϕ_{JL} (rad)	3.21	1.7
ϕ (rad)	3.98	5.03
RA (rad)	3.466	3.33
DEC (rad)	0.457	0.36
d_L (Mpc)	3310.9	849.5
ψ (rad)	1.61	2.64
θ_{JN} (rad)	1.38	1.57
t_{geo} (s)	1242442967.448563	1384782888.6267436
SNR	7.73	63.97

Due to the degeneracy between magnification and luminosity distance, it is first necessary to calculate the magnification for breaking this degeneracy. However, we are uncertain about the true luminosity distance d_L^l if the GW signal is lensed, so we cannot perform lens modeling. Owing to the existence of the PISN mass gap, Eq. (15) provides a lower mass bound of $m_{1,2}$ that in

² <https://git.ligo.org/lscsoft/bilby>

³ <https://gwosc.org>

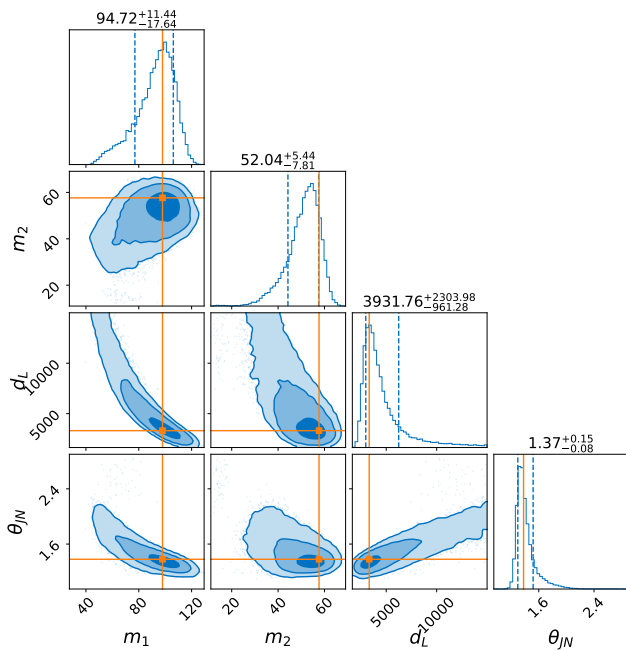


FIG. 3. Posterior distributions from the PE of a GW190521-like event using unlensed templates. The four parameters shown are the source-frame component masses m_1 , m_2 , the luminosity distance d_L and the angle θ_{jN} . The orange lines indicate the injection values (note that the injections were performed using the detector-frame masses; thus, the source-frame masses shown here are obtained by converting the injected detector-frame masses using the corresponding luminosity distance). The blue dashed lines indicate the 15.8% and 84.1% quantiles. The inferred primary mass m_1 lies within the mass gap.

turn constrains a corresponding lower limit of the source redshift. We can regard the luminosity distance associated with this redshift as the true luminosity distance d_L^l of the source after accounting for lensing magnification. Then, by comparing it with the luminosity distance d_L inferred without lensing, the required magnification can be obtained using Eq. (16). This approach does not rely on any specific lens model. Instead, it only considers the redshift necessary to ensure that the BBH masses in the source frame lies below the lower edge of the PISN mass gap, which is then translated into the corresponding lensing magnification effect. We present the source-frame BH mass corresponding to different values of magnification for the events GW190521 and GW231123, as shown in Fig. 2.

Finally, we performed Bayesian PE on the simulated signals using both lensed and unlensed GW waveforms. To reduce computational cost, we only considered four free parameters: detector-frame BBH masses $m_{1,2}^d$ with priors $U(10, 300) M_\odot$ and $U(10, 120) M_\odot$, respectively. Luminosity distance d_L with a $\alpha = 2$ power-law prior (10, 30000) Mpc. The angle θ_{jN} with a uniform prior (0, π) rad in sine. And the priors of other parameters is set to be their injection values shown in Tables I. For the

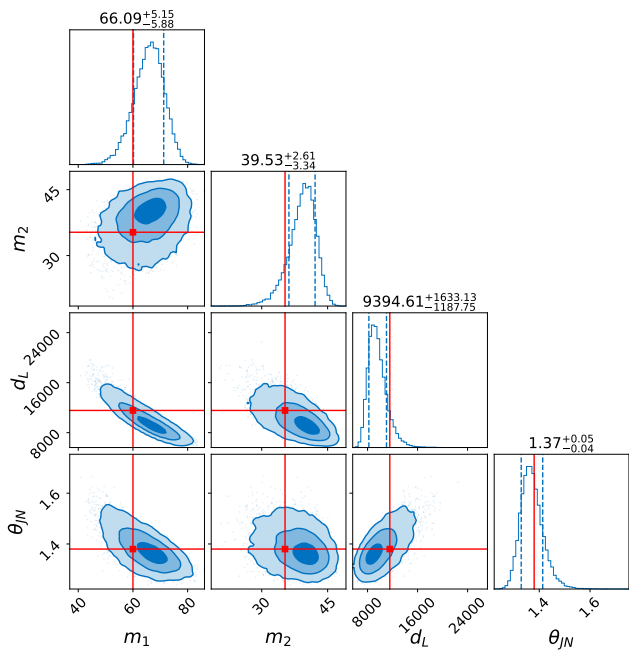


FIG. 4. Posterior distributions from the parameter estimation of a GW190521-like event using lensed templates with a magnification of $\mu = 12.2$. The four parameters shown are same to Fig. 3. The red lines indicate the predicted values through Eqs. (15) and (16) (except for θ_{jN}). By including the lensing effect, a larger luminosity distance is recovered, which in turn yields lower source-frame masses, bringing the primary mass close to the lower boundary of the mass gap.

prior of μ , we select a set of magnification factors referring to Fig. (1) for the lensed waveform. The corresponding PE results are presented in Tables II and III. For sampling, we use the built-in sampler **dynesty** [71, 72] in Bilby.

IV. RESULT

Whether or not the lensing effect is taken into account can significantly influence the inferred parameters of a GW source, potentially leading to the appearance of mass gap events like GW190521 and GW231123. In this section, we assess how lensing effect impacts four key parameters and under what conditions it can account for these unusual events.

When the magnification factor is equal to 1, it indicates that no lensing effect is present. As shown in Fig. 2, the source-frame BH masses and luminosity distances of the two events in this case correspond to the median values obtained from PE with unlensed templates in real situation. As the magnification increases, the source-frame masses gradually decrease, meaning that a sufficiently strong lensing system can indeed shift the masses out of the PISN mass gap, which also corresponds to a larger luminosity distance. According to Fig. 2, if we assume

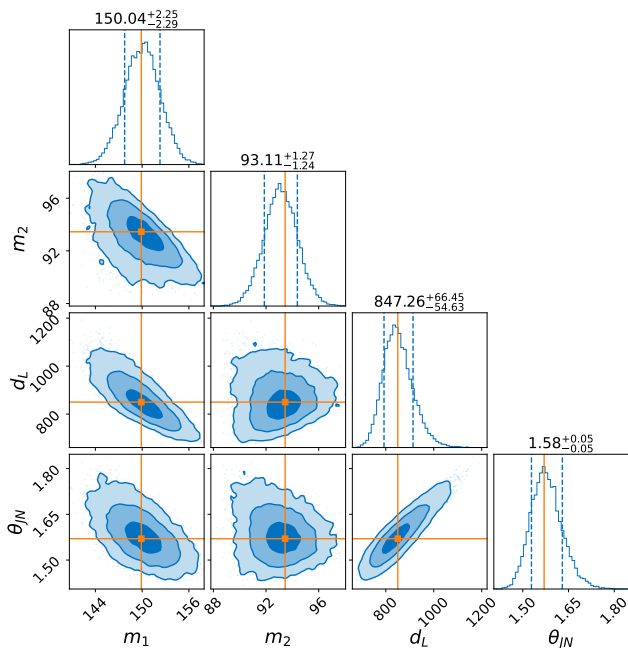


FIG. 5. Similar to Fig. 3, the posterior distributions from the PE of a GW231123-like event using unlensed templates are shown. Both m_1 and m_2 lie within the mass gap.

the lower boundary of the PISN mass gap to be $60 M_\odot$, then for GW190521 and GW231123, they would require lensing magnifications of at least $\mu = 12.2$ and $\mu = 320.1$, respectively, corresponding to lensing-corrected luminosity distances of 11155 Mpc and 15207 Mpc. Under such magnifications, their source-frame masses would fall below $60 M_\odot$, thereby moving out of the mass gap.

For the GW190521-like event, the posterior distributions obtained from PE using the unlensed template are shown in Fig. 3. It should be noted that in the PE results we do not directly obtain the posteriors of m_1 and m_2 . Instead, we first convert the posterior samples of d_L into redshift, and then use Eq. (15) to transform the inferred posteriors $m_{1,2}^d$ into $m_{1,2}$. The truth values (orange lines) in the marginal distributions are also obtained by applying the same procedure to convert the injected m_1^d and m_2^d . If we take the lower bound of the mass-gap interval to be $60 M_\odot$, we find that m_1 fall within the mass gap. When performing PE with the lensed GW template, as the result shown in Table II, we see that for $\mu = 8.7$, m_1 and m_2 decrease from their unlensed values of $94.72^{+11.44}_{-17.64} M_\odot$, $52.04^{+5.44}_{-7.81} M_\odot$ to $71.64^{+5.32}_{-6.36} M_\odot$, $39.20^{+2.70}_{-3.22} M_\odot$, respectively, while the luminosity distance increases from $3931.76^{+2303.98}_{-961.28}$ Mpc to $8231.03^{+1585.28}_{-1096.39}$ Mpc. As μ further increases to the maximum value 35.5, m_1 and m_2 decrease to its minimum values of $44.58^{+4.78}_{-3.63} M_\odot$ and $24.19^{+2.50}_{-2.75} M_\odot$, with the luminosity distance reaching its maximum of $21202.27^{+2526.98}_{-2940.92}$ Mpc.

Based on the results of Fig. 2, when $\mu = 12.2$, the inferred source-frame masses are expected to lie near

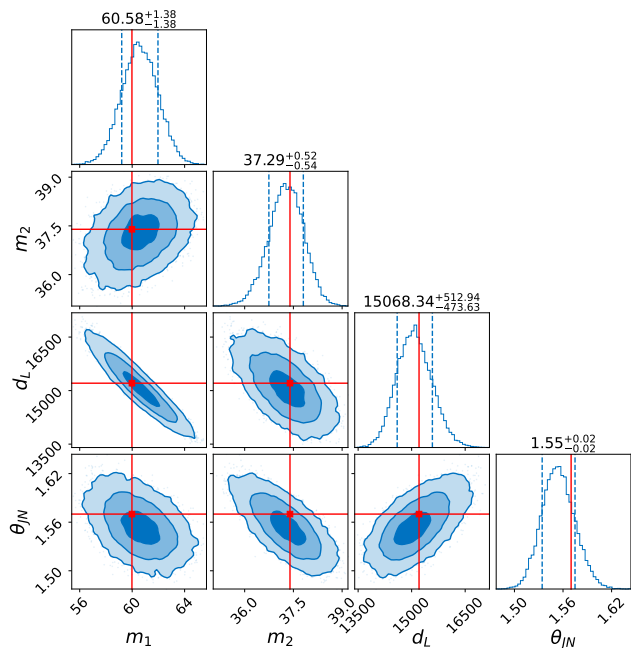


FIG. 6. Similar to Fig. 5, posterior distributions from the PE of a GW231123-like event using lensed templates with a magnification of $\mu = 320.1$. By including the lensing effect, a larger luminosity distance is recovered, which consequently shifts the source-frame masses above the lower boundary of the mass gap.

$60 M_\odot$. However, this is inconsistent with our PE results: only when $\mu = 17.2$ do we obtain $m_1 = 61.20^{+5.08}_{-5.71} M_\odot$, which is close to exiting the mass gap. The PE result for $\mu = 12.2$ is shown in Fig. 4. The red lines (except for θ_{JN} , which shows the injected value) represent the predicted values obtained from Eqs. (15) and (15) for the given magnification μ . The inferred source-frame mass of the primary black hole is $66.09^{+5.15}_{-5.88} M_\odot$, significantly higher than the predicted $60 M_\odot$ (red line). The mass of the secondary black hole is also considerably higher than the corresponding predicted value ($35 M_\odot$). This discrepancy arises from a bias in the estimation of the luminosity distance: the PE result yields $d_L = 9394.61^{+1633.13}_{-1187.75}$ Mpc, which is smaller than the predicted value indicated by the red line ($d_L = 11155$ Mpc). When using the lensed templates, the detector-frame masses are recovered accurately, but the underestimated d_L leads to an overestimation of the source-frame masses. Moreover, this bias in the luminosity distance persists regardless of the value of μ shown in Tables II, preventing us from fully recovering the true source-frame masses. This is because the GW190521-like event has a relatively low SNR, which affects the PE results. For such low-SNR events, even when the lensing magnification is taken into account, the strong noise contamination can still lead to a biased estimate of the luminosity distance in the PE, thereby hindering the recovery of the true luminosity distance. As a result, one may reach an incorrect conclusion: for ex-

TABLE II. PE results of GW190521-like events using lensed template with different prior values of magnifications μ .

GW190521-like						
μ	35.5	24.5	17.2	12.2	8.7	1 (unlensed)
$m_1 (M_\odot)$	$44.58^{+4.78}_{-3.63}$	$55.55^{+5.52}_{-4.86}$	$61.20^{+5.08}_{-5.71}$	$66.09^{+5.15}_{-5.88}$	$71.64^{+5.32}_{-6.36}$	$94.72^{+11.44}_{-17.64}$
$m_2 (M_\odot)$	$24.19^{+2.50}_{-2.75}$	$24.41^{+2.74}_{-2.56}$	$33.44^{+2.55}_{-2.89}$	$39.53^{+2.61}_{-3.34}$	$39.20^{+2.70}_{-3.22}$	$52.04^{+5.44}_{-7.81}$
d_L^l (Mpc)	$21202.27^{+2526.98}_{-2940.92}$	$15733^{+2558.60}_{-2367.96}$	$11568.85^{+2108.19}_{-1552.77}$	$9394.61^{+1633.13}_{-1187.75}$	$8231.03^{+1585.28}_{-1096.39}$	$3931.76^{+2303.98}_{-961.28}$
θ_{JN} (rad)	$1.40^{+0.05}_{-0.05}$	$1.30^{+0.06}_{-0.06}$	$1.32^{+0.04}_{-0.03}$	$1.37^{+0.05}_{-0.04}$	$1.32^{+0.04}_{-0.03}$	$1.37^{+0.15}_{-0.08}$

TABLE III. Similar to the results shown in Table II, PE results of GW231123-like events.

GW231123-like						
μ	864.6	610.3	438.8	320.1	236.1	1 (unlensed)
$m_1 (M_\odot)$	$43.31^{+0.96}_{-0.97}$	$48.18^{+1.02}_{-1.02}$	$56.04^{+1.03}_{-1.05}$	$60.58^{+1.38}_{-1.38}$	$66.15^{+1.13}_{-1.15}$	$150.04^{+2.25}_{-2.29}$
$m_2 (M_\odot)$	$27.63^{+0.41}_{-0.43}$	$30.74^{+0.45}_{-0.46}$	$34.05^{+0.44}_{-0.46}$	$37.29^{+0.52}_{-0.54}$	$40.20^{+0.49}_{-0.50}$	$93.11^{+1.27}_{-1.24}$
d_L^l (Mpc)	$26192.94^{+729.61}_{-703.77}$	$22008.14^{+614.80}_{-582.25}$	$17428.75^{+455.00}_{-443.69}$	$15068.34^{+512.94}_{-473.63}$	$12782.11^{+333.94}_{-322.47}$	$847.26^{+66.45}_{-54.63}$
θ_{JN} (rad)	$1.58^{+0.02}_{-0.02}$	$1.58^{+0.02}_{-0.02}$	$1.57^{+0.02}_{-0.02}$	$1.55^{+0.02}_{-0.02}$	$1.57^{+0.02}_{-0.02}$	$1.58^{+0.05}_{-0.05}$

ample, although the predicted requirement is a lensing magnification of $\mu = 12.2$ to explain a GW190521-like mass gap event, the PE result instead suggests that a larger magnification is needed.

For the GW231123-like event, if we require its source-frame masses to lie below the lower edge of the mass gap, a larger lensing magnification is needed because its detector-frame masses are higher than GW190521-like event. The posterior distributions obtained from PE with the unlensed template are shown in Fig. 5. If we take the lower bound of the mass-gap interval to be $60 M_\odot$, we find that both m_1 and m_2 fall within the mass gap, with the source located at a luminosity distance of $847.26^{+66.45}_{-54.63}$ Mpc. When performing PE with the lensed GW template, as the result shown in Table III, we see that for $\mu = 236.1$, m_1 and m_2 decrease from their unlensed values of $150.04^{+2.25}_{-2.29} M_\odot$, $93.11^{+1.27}_{-1.24} M_\odot$ to $66.15^{+1.13}_{-1.15} M_\odot$, $40.20^{+0.49}_{-0.50} M_\odot$, respectively, while the luminosity distance increases to $12782.11^{+333.94}_{-322.47}$ Mpc. As μ further increases to the maximum value 864.6, m_1 and m_2 decrease to minimum values of $43.31^{+0.96}_{-0.97} M_\odot$ and $27.63^{+0.41}_{-0.43} M_\odot$, with the luminosity distance reaching its maximum of $26192.94^{+729.61}_{-703.77}$ Mpc. Moreover, due to its high SNR, the PE results are very accurate and do not exhibit the kind of bias in the luminosity distance seen in the GW190521-like event. Therefore, if we attempt to interpret GW231123 falling into the mass gap ($m > 60 M_\odot$) by invoking lensing effects, the required magnification is at least 320.1, with the PE results shown in Fig. 6. The true luminosity distance of the source is $15068.34^{+512.94}_{-473.63}$ Mpc. At this point, we find

$m_1 = 60.58^{+1.38}_{-1.38} M_\odot$ and $m_2 = 37.29^{+0.52}_{-0.54} M_\odot$, both lying outside the lower edge of the mass gap.

V. SUMMARY AND DISCUSSION

In this work, we discuss the possibility of explaining gravitational wave (GW) from binary black hole (BBH) merger located within the pair-instability supernova (PISN) mass gap by considering the effects of gravitational lensing. First, we describe how to construct lensed GW waveform templates under the geometric-optics approximation. Then, we introduce the Bayesian parameter estimation (PE) method. In the PE process, the construction of the likelihood function is crucial, whether lensing effects are considered or not leads to different forms of the likelihood function, thereby affecting the resulting posterior samples. Specifically, the source-frame masses of black holes are related to their detector-frame masses through the redshift. If the GW signal is lensed, using an unlensed waveform template will lead to an underestimation of the luminosity distance, which in turn biases the inferred redshift and ultimately results in an overestimation of the source-frame masses. Therefore, for high-mass GW events such as GW190521 and GW231123, one possible explanation for their inferred source-frame masses falling into the PISN mass gap is the influence of gravitational lensing, which has not been accounted for in standard PE analyses.

To recover the intrinsic masses and luminosity distances that were misestimated due to the neglect of lensing effects, we simulate GW190521-like and GW231123-

like signals and inject them into the LIGO-Virgo-KAGRA (LVK) network. We then perform Bayesian PE using both unlensed and lensed waveform templates, taking the detector-frame BBH masses $m_{1,2}^d$, luminosity distance d_L and the angle between line of sight and the total angular momentum θ_{JN} as free parameters. For different assumed lower boundaries of the mass gap, we determine the magnification factors required for the binary masses to move out of the mass gap, thereby breaking the degeneracy between magnification and luminosity distance. When using the lensed waveform templates, for the GW190521-like event, assuming a mass-gap lower boundary of $60 M_{\odot}$, that is, requiring the source-frame masses to be below than it, the lens with a magnification of at least $\mu = 17.2$ is required, corresponding to a true luminosity distance of approximately $11568.85_{-1552.77}^{+2108.19}$ Mpc. However, because the SNR is low, this estimate is inaccurate. In reality, only a magnification of $\mu = 12.2$ is required, in which case the source would be located at 11155 Mpc. And for the GW231123-like event, a lensing system with $\mu = 320.1$ is needed, corresponding to a true luminosity distance of approximately $15068.34_{-473.63}^{+512.94}$ Mpc, consistent with our expected value 15207 Mpc.

The bias in the estimation for low-SNR events is expected to be resolved with third-generation detectors such as the Einstein Telescope (ET) [73] or Cosmic Explorer (CE) [74]. Their sensitivities are anticipated to be about two orders of magnitude higher than the cur-

rent instruments, enabling much higher SNRs in detections. A higher SNR leads to significantly improved PE performance. As demonstrated by the GW231123-like event, the true source mass and luminosity distance can be accurately recovered when lensing effects are taken into account. Moreover, during the current LVK observing runs, the detection of lensed BBH signals is almost impossible [75, 76]. However, with the operation of future third-generation detectors, the number of detected lensed events could reach hundreds [77, 78], and we may also observe many more high-mass GW events. Therefore, Bayesian inference of source-frame masses under the lensing scenario will provide an alternative way to interpret high-mass BBH GW events that appear to reside within the PISN mass gap.

ACKNOWLEDGMENTS

We thank Mingqi Sun for useful discussion. You, Z.-Q. is supported by the National Natural Science Foundation of China (Grant No. 12305059); The Startup Research Fund of Henan Academy of Sciences (No. 241841224); The Scientific and Technological Research Project of Henan Academy of Science (No. 20252345003); Joint Fund of Henan Province Science and Technology R&D Program (No. 235200810111); Henan Province High-Level Talent Internationalization Cultivation Program (No. 2024032).

-
- [1] LIGO Scientific Collaboration and Virgo Collaboration, *Classical and Quantum Gravity* **32**, 074001 (2015), [arXiv:1411.4547 \[gr-qc\]](#).
 - [2] LIGO Scientific Collaboration and Virgo Collaboration, *Phys. Rev. D* **93**, 122003 (2016), [arXiv:1602.03839 \[gr-qc\]](#).
 - [3] LIGO Scientific Collaboration and Virgo Collaboration, *Phys. Rev. Lett.* **116**, 061102 (2016), [arXiv:1602.03837 \[gr-qc\]](#).
 - [4] LIGO Scientific Collaboration and Virgo Collaboration, *Phys. Rev. Lett.* **116**, 131103 (2016), [arXiv:1602.03838 \[gr-qc\]](#).
 - [5] Virgo Collaboration, *Classical and Quantum Gravity* **32**, 024001 (2015), [arXiv:1408.3978 \[gr-qc\]](#).
 - [6] K. Somiya, *Classical and Quantum Gravity* **29**, 124007 (2012), [arXiv:1111.7185 \[gr-qc\]](#).
 - [7] Y. Aso, Y. Michimura, K. Somiya, M. Ando, O. Miyakawa, T. Sekiguchi, D. Tatsumi, and H. Yamamoto, *Phys. Rev. D* **88**, 043007 (2013), [arXiv:1306.6747 \[gr-qc\]](#).
 - [8] Kagra Collaboration, *Nature Astronomy* **3**, 35 (2019), [arXiv:1811.08079 \[gr-qc\]](#).
 - [9] Kagra Collaboration, *Progress of Theoretical and Experimental Physics* **2021**, 05A102 (2021), [arXiv:2009.09305 \[gr-qc\]](#).
 - [10] LIGO Scientific Collaboration and Virgo Collaboration, *Physical Review X* **9**, 031040 (2019), [arXiv:1811.12907 \[astro-ph.HE\]](#).
 - [11] LIGO Scientific Collaboration and Virgo Collaboration, *Physical Review X* **11**, 021053 (2021), [arXiv:2010.14527 \[gr-qc\]](#).
 - [12] LIGO Scientific Collaboration and Virgo Collaboration, *Physical Review X* **13**, 041039 (2023), [arXiv:2111.03606 \[gr-qc\]](#).
 - [13] The LIGO Scientific Collaboration and the Virgo Collaboration and the KAGRA Collaboration, *arXiv e-prints*, [arXiv:2508.18081 \(2025\)](#), [arXiv:2508.18081 \[gr-qc\]](#).
 - [14] LIGO Scientific Collaboration and Virgo Collaboration, *Phys. Rev. Lett.* **125**, 101102 (2020), [arXiv:2009.01075 \[gr-qc\]](#).
 - [15] LIGO Scientific Collaboration and Virgo Collaboration, *Astrophysical Journal Letter* **900**, L13 (2020), [arXiv:2009.01190 \[astro-ph.HE\]](#).
 - [16] LIGO Scientific Collaboration and Virgo Collaboration, *Phys. Rev. D* **109**, 022001 (2024), [arXiv:2108.01045 \[gr-qc\]](#).
 - [17] W. A. Fowler and F. Hoyle, *Astrophysical Journal Supplement* **9**, 201 (1964).
 - [18] A. Heger and S. E. Woosley, *Astrophysical Journal* **567**, 532 (2002), [arXiv:astro-ph/0107037 \[astro-ph\]](#).
 - [19] A. Heger and S. E. Woosley, *Astrophysical Journal* **724**, 341 (2010), [arXiv:0803.3161 \[astro-ph\]](#).
 - [20] K. Belczynski, A. Heger, W. Gladysz, A. J. Ruiter, S. Woosley, G. Wiktorowicz, H.-Y. Chen, T. Bulik, R. O’Shaughnessy, D. E. Holz, C. L. Fryer, and E. Berti, *Astronomy & Astrophysics* **594**, A97 (2016),

- arXiv:1607.03116 [astro-ph.HE].
- [21] S. E. Woosley, *Astrophysical Journal* **836**, 244 (2017), arXiv:1608.08939 [astro-ph.HE].
- [22] R. Farmer, M. Renzo, S. E. de Mink, P. Marchant, and S. Justham, *Astrophysical Journal* **887**, 53 (2019), arXiv:1910.12874 [astro-ph.SR].
- [23] S.-C. Leung, S. Blinnikov, K. Ishidoshiro, A. Kozlov, and K. Nomoto, *Astrophysical Journal* **889**, 75 (2020), arXiv:2007.08470 [astro-ph.HE].
- [24] P. Marchant and T. J. Moriya, *Astronomy & Astrophysics* **640**, L18 (2020), arXiv:2007.06220 [astro-ph.HE].
- [25] M. Renzo, R. J. Farmer, S. Justham, S. E. de Mink, Y. Götberg, and P. Marchant, *Monthly Notices of the Royal Astronomical Society* **493**, 4333 (2020), arXiv:2002.08200 [astro-ph.SR].
- [26] A. Ray and V. Kalogera, arXiv e-prints , arXiv:2510.18867 (2025), arXiv:2510.18867 [astro-ph.HE].
- [27] F. Antonini, I. Romero-Shaw, T. Callister, F. Dosopoulou, D. Chattopadhyay, M. Gieles, and M. Mapelli, arXiv e-prints , arXiv:2509.04637 (2025), arXiv:2509.04637 [astro-ph.HE].
- [28] S. Afroz and S. Mukherjee, arXiv e-prints , arXiv:2509.09123 (2025), arXiv:2509.09123 [astro-ph.HE].
- [29] M. Fishbach and D. E. Holz, *Astrophysical Journal Letter* **904**, L26 (2020), arXiv:2009.05472 [astro-ph.HE].
- [30] E. Farrell, J. H. Groh, R. Hirschi, L. Murphy, E. Kaiser, S. Ekström, C. Georgy, and G. Meynet, *Monthly Notices of the Royal Astronomical Society* **502**, L40 (2021), arXiv:2009.06585 [astro-ph.SR].
- [31] The LIGO Scientific Collaboration and the Virgo Collaboration and the KAGRA Collaboration, *Astrophysical Journal Letter* **993**, L25 (2025), arXiv:2507.08219 [astro-ph.HE].
- [32] I. Magaña Hernandez and A. Palmese, arXiv e-prints , arXiv:2508.19208 (2025), arXiv:2508.19208 [astro-ph.HE].
- [33] V. De Luca, V. Desjacques, G. Franciolini, P. Pani, and A. Riotto, *Phys. Rev. Lett.* **126**, 051101 (2021), arXiv:2009.01728 [astro-ph.CO].
- [34] S. Clesse and J. García-Bellido, *Physics of the Dark Universe* **38**, 101111 (2022), arXiv:2007.06481 [astro-ph.CO].
- [35] Z.-C. Chen, C. Yuan, and Q.-G. Huang, *Physics Letters B* **829**, 137040 (2022), arXiv:2108.11740 [astro-ph.CO].
- [36] G. Franciolini, V. Baibhav, V. De Luca, K. K. Y. Ng, K. W. K. Wong, E. Berti, P. Pani, A. Riotto, and S. Vitale, *Phys. Rev. D* **105**, 083526 (2022), arXiv:2105.03349 [gr-qc].
- [37] V. De Luca, G. Franciolini, and A. Riotto, arXiv e-prints , arXiv:2508.09965 (2025), arXiv:2508.09965 [astro-ph.CO].
- [38] C. Yuan, Z.-C. Chen, and L. Liu, *Phys. Rev. D* **112**, L081306 (2025), arXiv:2507.15701 [astro-ph.CO].
- [39] B. Liu and D. Lai, *Monthly Notices of the Royal Astronomical Society* **502**, 2049 (2021), arXiv:2009.10068 [astro-ph.HE].
- [40] M. Mapelli, M. Dall’Amico, Y. Bouffanais, N. Giacobbo, M. Arca Sedda, M. C. Artale, A. Ballone, U. N. Di Carlo, G. Iorio, F. Santoliquido, and S. Tornamenti, *Monthly Notices of the Royal Astronomical Society* **505**, 339 (2021), arXiv:2103.05016 [astro-ph.HE].
- [41] O. Anagnostou, M. Trenti, and A. Melatos, *Astrophysical Journal* **941**, 4 (2022), arXiv:2010.06161 [astro-ph.HE].
- [42] C. Araújo-Álvarez, H. W. Y. Wong, A. Liu, and J. Calderón Bustillo, *Astrophysical Journal* **977**, 220 (2024), arXiv:2404.00720 [astro-ph.HE].
- [43] G.-P. Li and X.-L. Fan, arXiv e-prints , arXiv:2509.08298 (2025), arXiv:2509.08298 [astro-ph.HE].
- [44] Y.-J. Li, S.-P. Tang, L.-Q. Xue, and Y.-Z. Fan, arXiv e-prints , arXiv:2507.17551 (2025), arXiv:2507.17551 [astro-ph.HE].
- [45] L. Passenger, S. Banagiri, E. Thrane, P. D. Lasky, A. Borchers, M. Fishbach, and C. S. Ye, arXiv e-prints , arXiv:2510.14363 (2025), arXiv:2510.14363 [astro-ph.HE].
- [46] L. Paiella, C. Ugolini, M. Spera, M. Branchesi, and M. Arca Sedda, arXiv e-prints , arXiv:2509.10609 (2025), arXiv:2509.10609 [astro-ph.GA].
- [47] Y. Ali-Haïmoud, E. D. Kovetz, and M. Kamionkowski, *Phys. Rev. D* **96**, 123523 (2017), arXiv:1709.06576 [astro-ph.CO].
- [48] M. Raidal, V. Vaskonen, and H. Veermäe, arXiv e-prints , arXiv:2404.08416 (2024), arXiv:2404.08416 [astro-ph.CO].
- [49] D. Gerosa and M. Fishbach, *Nature Astronomy* **5**, 749 (2021), arXiv:2105.03439 [astro-ph.HE].
- [50] P. Mahapatra, A. Gupta, M. Favata, K. G. Arun, and B. S. Sathyaprakash, *Astrophysical Journal Letter* **918**, L31 (2021), arXiv:2106.07179 [astro-ph.HE].
- [51] M. Fishbach, C. Kimball, and V. Kalogera, *Astrophysical Journal Letter* **935**, L26 (2022), arXiv:2207.02924 [astro-ph.HE].
- [52] S. Tornamenti, M. Mapelli, C. Périgois, M. Arca Sedda, M. C. Artale, M. Dall’Amico, and M. P. Vaccaro, *Astronomy & Astrophysics* **688**, A148 (2024), arXiv:2401.14837 [astro-ph.HE].
- [53] T. Broadhurst, J. M. Diego, and G. F. Smoot, arXiv e-prints , arXiv:2002.08821 (2020), arXiv:2002.08821 [gr-qc].
- [54] X. Shan, H. Yang, S. Mao, and O. A. Hannuksela, arXiv e-prints , arXiv:2508.21262 (2025), arXiv:2508.21262 [astro-ph.CO].
- [55] M. Oguri, *Monthly Notices of the Royal Astronomical Society* **480**, 3842 (2018), arXiv:1807.02584 [astro-ph.CO].
- [56] S.-S. Li, S. Mao, Y. Zhao, and Y. Lu, *Monthly Notices of the Royal Astronomical Society* **476**, 2220 (2018), arXiv:1802.05089 [astro-ph.CO].
- [57] A. Robertson, G. P. Smith, R. Massey, V. Eke, M. Jauzac, M. Bianconi, and D. Ryczanowski, *Monthly Notices of the Royal Astronomical Society* **495**, 3727 (2020), arXiv:2002.01479 [astro-ph.CO].
- [58] D. Ryczanowski, G. P. Smith, M. Bianconi, R. Massey, A. Robertson, and M. Jauzac, *Monthly Notices of the Royal Astronomical Society* **495**, 1666 (2020), arXiv:2005.02296 [astro-ph.GA].
- [59] L. Dai, T. Venumadhav, and K. Sigurdson, *Phys. Rev. D* **95**, 044011 (2017), arXiv:1605.09398 [astro-ph.CO].
- [60] K. K. Y. Ng, K. W. K. Wong, T. Broadhurst, and T. G. F. Li, *Phys. Rev. D* **97**, 023012 (2018), arXiv:1703.06319 [astro-ph.CO].
- [61] P. T. H. Pang, O. A. Hannuksela, T. Dietrich, G. Pagano, and I. W. Harry, *Monthly Notices of the Royal Astronomical Society* **495**, 3740 (2020), arXiv:2002.04893 [astro-ph.HE].
- [62] Planck Collaboration, *Astronomy & Astrophysics* **641**, A6 (2020), arXiv:1807.06209 [astro-ph.CO].
- [63] Astropy Collaboration, *Astrophysical Journal* **935**, 167

- (2022), [arXiv:2206.14220 \[astro-ph.IM\]](#).
- [64] P. Schneider, J. Ehlers, and E. E. Falco, *Gravitational Lenses* (1992).
- [65] T. T. Nakamura and S. Deguchi, *Progress of Theoretical Physics Supplement* **133**, 137 (1999).
- [66] R. Takahashi and T. Nakamura, *Astrophysical Journal* **595**, 1039 (2003), [arXiv:astro-ph/0305055 \[astro-ph\]](#).
- [67] G. Ashton, M. Hübner, P. D. Lasky, C. Talbot, K. Ackley, S. Biscoveanu, Q. Chu, A. Divakarla, P. J. Easter, B. Goncharov, F. Hernandez Vivanco, J. Harms, M. E. Lower, G. D. Meadors, D. Melchor, E. Payne, M. D. Pitkin, J. Powell, N. Sarin, R. J. E. Smith, and E. Thrane, *Astrophysical Journal Supplement* **241**, 27 (2019), [arXiv:1811.02042 \[astro-ph.IM\]](#).
- [68] S. Khan, K. Chatzioannou, M. Hannam, and F. Ohme, *Phys. Rev. D* **100**, 024059 (2019), [arXiv:1809.10113 \[gr-qc\]](#).
- [69] G. Pratten, C. García-Quirós, M. Colleoni, A. Ramos-Buades, H. Estellés, M. Mateu-Lucena, R. Jaume, M. Haney, D. Keitel, J. E. Thompson, and S. Husa, *Phys. Rev. D* **103**, 104056 (2021), [arXiv:2004.06503 \[gr-qc\]](#).
- [70] The LIGO Scientific Collaboration and the Virgo Collaboration and the KAGRA Collaboration, [arXiv e-prints](#), [arXiv:2508.18079 \(2025\)](#), [arXiv:2508.18079 \[gr-qc\]](#).
- [71] J. S. Speagle, *Monthly Notices of the Royal Astronomical Society* **493**, 3132 (2020), [arXiv:1904.02180 \[astro-ph.IM\]](#).
- [72] S. Kaposov, J. Speagle, K. Barbary, G. Ashton, E. Bennett, J. Buchner, C. Scheffler, C. Talbot, B. Cook, J. Guillochon, P. Cubillos, A. A. Ramos, M. Dartiailh, Ilya, E. Tollerud, D. Lang, B. Johnson, jtmendel, E. Higson, T. Vandal, T. Daylan, R. Angus, patelR, P. Cargile, P. Sheehan, M. Pitkin, M. Kirk, L. Xu, J. Leja, and joezuntz, [joshspeagle/dynesty: v3.0.0 \(2025\)](#).
- [73] M. Maggiore, C. Van Den Broeck, N. Bartolo, E. Belgacem, D. Bertacca, M. A. Bizouard, M. Branchesi, S. Clesse, S. Foffa, J. García-Bellido, S. Grimm, J. Harms, T. Hinderer, S. Matarrese, C. Palomba, M. Peloso, A. Ricciardone, and M. Sakellariadou, *JCAP* **2020** (3), 050, [arXiv:1912.02622 \[astro-ph.CO\]](#).
- [74] D. Reitze, R. X. Adhikari, S. Ballmer, B. Barish, L. Barsotti, G. Billingsley, D. A. Brown, Y. Chen, D. Coyne, R. Eisenstein, M. Evans, P. Fritschel, E. D. Hall, A. Lazzarini, G. Lovelace, J. Read, B. S. Sathyaprakash, D. Shoemaker, J. Smith, C. Torrie, S. Vitale, R. Weiss, C. Wipf, and M. Zucker, in *Bulletin of the American Astronomical Society*, Vol. 51 (2019) p. 35, [arXiv:1907.04833 \[astro-ph.IM\]](#).
- [75] J. Janquart, M. Wright, S. Goyal, J. C. L. Chan, A. Ganguy, Á. Garrón, D. Keitel, A. K. Y. Li, A. Liu, R. K. L. Lo, A. Mishra, A. More, H. Phurailatpam, P. Prasia, P. Ajith, S. Biscoveanu, P. Cremonese, J. R. Cudell, J. M. Ezquiaga, J. Garcia-Bellido, O. A. Hannuksela, K. Haris, I. Harry, M. Hendry, S. Husa, S. Kapadia, T. G. F. Li, I. Magaña Hernandez, S. Mukherjee, E. Seo, C. Van Den Broeck, and J. Veitch, *Monthly Notices of the Royal Astronomical Society* **526**, 3832 (2023), [arXiv:2306.03827 \[gr-qc\]](#).
- [76] LIGO Scientific Collaboration and Virgo Collaboration, *Astrophysical Journal* **970**, 191 (2024), [arXiv:2304.08393 \[gr-qc\]](#).
- [77] X. Ding, M. Biesiada, and Z.-H. Zhu, *JCAP* **2015** (12), 006, [arXiv:1508.05000 \[astro-ph.HE\]](#).
- [78] Z. Gao, K. Liao, L. Yang, and Z.-H. Zhu, *Monthly Notices of the Royal Astronomical Society* **526**, 682 (2023), [arXiv:2304.13967 \[astro-ph.IM\]](#).